Revista de I+D TECNOLÓGICO
Portal de revistas: http://revistas.utp.ac.pa

TCAD 2D numerical simulations for increasing efficiency of AlGaAs – GaAs Solar Cells

Simulaciones numéricas TCAD en 2D para mejorar la eficiencia de celdas solares basadas en AlGaAs - GaAs

César A. Palacios A. [1*], Noemi Guerra[2], Marco Guevara[3], María José López[4]

[1] *Facultad de Ingeniería, Universidad Nacional de Chimborazo, Ecuador*
[2] *Departamento de Investigación, Universidad Tecnológica de Panamá, Panamá*
[3] *Facultad de Mecánica, Escuela Superior Politécnica de Chimborazo, Ecuador*
[4] *Facultad de Ciencias Pecuarias, Escuela Superior Politécnica de Chimborazo, Ecuador*
***Autor de correspondencia:** cesar.palacios@unach.edu.ec

ABSTRACT– The performance of solar cells has improved quickly in recent years, the latest research focuses on thin cells, multijunction cells, solar cells of the group III-V compounds, Tandem cells, etc. In the present work, numerical simulations are developed, using SENTAURUS TCAD as a tool, in order to obtain a solar cell model based on Galium Arsenide (GaAs). This solar cell corresponds to the so-called "Thin Films" due to the fact that can make layers thinner than we would have if we work with conventional semiconductors, such as; Silicon or Germanium; thus opening the possibility of placing the cell as a top layer within a tandem solar cell configuration with compounds of group III-V. That is why two types of simulations are performed with respect to the contact of the rear contact; one corresponds to the cell with a lower contact equal to the length of the cell and the other with a small contact of 5 µm. In addition, the cell undergoes an optimization process by modifying the geometry and doping of the layers that comprise it, in order to improve its performance. To achieve this objective, the initial conditions and the appropriate simulation parameters must be determined, which have been selected and corroborated with the literature, allowing us to arrive at coherent results and optimal models of solar cell design through numerical simulations.

Keywords– *Solar cells, AlGaAs-GaAs, solar energy, numerical simulations, TCAD, Sentaurus, optical simulation, electrical simulation.*

RESUMEN– Las prestaciones de las celdas solares han mejorado rápidamente en los últimos años, las últimas investigaciones se centran en las celdas delgadas (thin films), celdas multijunction, celdas solares con compuestos del grupo III-V, celdas tipo Tandem, etc. En el presente trabajo, se desarrollan simulaciones numéricas, usando SENTAURUS TCAD como herramienta, con el fin de obtener un modelo de celda solar basada en Arseniuro de Galio (GaAs), esta celda solar corresponde a las denominadas "Thin Films" debido a que se pueden realizar capas mucho más delgadas que las que tendríamos si trabajamos con semiconductores convencionales, como; Silicio o Germanio; abriendo así la posibilidad de colocar a la celda como una capa superior dentro de una configuración de celda solar tipo Tandem con compuestos del grupo III-V. Es por ello que se realizan dos tipos de simulaciones respecto al contacto de la parte inferior; una corresponde a la celda con un contacto inferior igual a la longitud de la celda y la otra con un contacto pequeño de 5 µm. Además, la celda se somete a un proceso de optimización mediante la modificación de la geometría y el dopaje de las capas que la conforman, con el fin de mejorar su rendimiento. Para poder lograr este objetivo se deben determinar las condiciones iniciales y los parámetros de simulación adecuados, los cuales han sido seleccionados y corroborados con la literatura, permitiéndonos llegar a resultados coherentes y modelos óptimos de diseño de celdas solares mediante simulaciones numéricas.

Palabras clave– *Celdas solares, AlGaAs-GaAs, energía solar, simulaciones numéricas, TCAD, Sentaurus, simulación óptica, simulación eléctrica.*

1. Introduction

The Sun is a big fusion reactor, it consists mainly of four hydrogen atoms melted into one helium atom. In the center of the Sun the pressure–temperature conditions are such that nuclear fusion can take place. The fusion temperatures in this process are around 15 million degrees Celsius [1]. Some characteristics of Sun are summarized on table 1.

1.1 Solar Radiation

Every hot body gives off radiation to its surroundings, according to Planck's Law of Radiation. The amount of power continuously radiated by the sun is $P_{Sun}=3{,}845\text{x}10^{26}W$, but the Earth only receives a small fraction [2]. To calculate this value, we assumes there is

Citación: C. Palacios, N. Guerra, M. Guevara y M. López, "TCAD 2D numerical simulations for increasing efficiency of AlGaAs – GaAs Solar Cells", *Revista de I+D Tecnológico*, vol. 14, no. 2, pp. (96-107), 2018.
Tipo de artículo: Original. **Recibido:** 21 de agosto de 2018. **Recibido con correcciones:** 12 de noviembre de 2018. **Aceptado:** 12 de noviembre de 2018.

a sphere around the Sun with a radius $r = d_{SE}$, as shown in figure 1.

Table 1. Characteristics of the sun [3]

Properties	Values
Diameter	$D_{Sun}=1{,}3\ x10^6\ km.$
Mass	$m_S=1933\ x\ 10^{27}\ Kg$
Surface temperature	$T_{Sun}=5578\ K$
Temperature at center	$15000000\ K$
Energy radiation	$P_{Sun}=3845\ x\ 1026\ W$
Mean distance Sun-Earth	$d_{SE}=149600000\ Km$

At the position of the Earth, the power density can be calculated as shown in Equation 1. The result of *1367* $W.m^{-2}$ denotes the irradiance outside the Earth's atmosphere and it is called the solar constant.

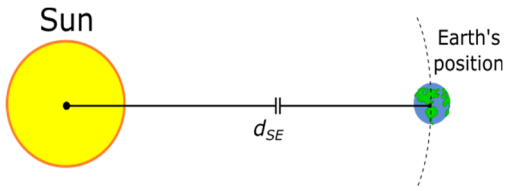

Figure 1. Solar radiation at the Earth's position

$$I_0 = \frac{P_{sun}}{A} = \frac{P_{sun}}{4.\pi.d_{SE}^2} \quad (1)$$

This value can be measured outside the Earth's atmosphere on a surface perpendicular to the solar radiation.

1.2 Solar spectrum

The solar spectrum denotes the composition of the light and the variation of the total irradiance due to the wavelengths. The typical measured values of radiation are usually lower than the solar constant, due to some factors of the atmosphere, as reflection of light by the atmosphere, absorption in the atmosphere (mainly O_3, H_2, O, O_2 and CO_2), Rayleigh scattering and Mie scattering [4].

The absorption of light is selective and affects only some parts of the spectrum, is caused by the presence of different gases in the atmosphere, like water vapor, ozone and carbon dioxide. Ozone absorbs radiation with wavelengths below 300nm. Raylengh scattering is provoked by the presence of molecular air particles with diameters smaller than the wavelength of light. Shorter the light wavelength grater the Rayleigh scattering. Mie scattering, in the other hand, is caused by dust particles and air pollution. In this case, the diameter of the particles is larger than the wavelength of light. Mie scattering changes with the location, there is one type of scattering at mountains and there is a different for industrial regions [5].

The most important factor that determines the solar irradiance is the distance that sunlight has to travel though the atmosphere. When the sun is at the zenith, the distance is the shortest. The ratio of a path length of the sunlight to this minimal distance is known as the Optical Air Mass [6]. Thus, the effect is greater, longer is the path of the light. When the sun is at its zenith the optical air mass is unity an the spectrum is called the air mass 1 (AM1) spectrum, as shown in figure 2. When the sun is at a different angle with the zenith, the air mass is given by equation 2.

$$AM = \frac{1}{cos(\theta)} \quad (2)$$

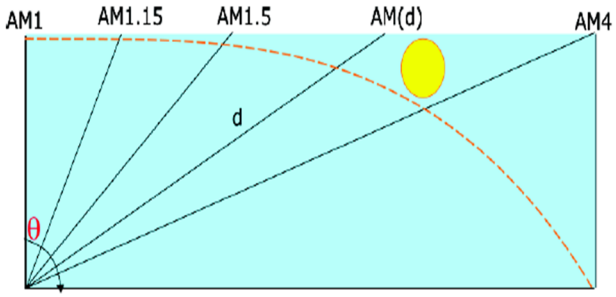

Figure 2. Air mass as a function of θ angle.

In an easier way, we can say that the term AM 1.5 means the light has traveled 1.5 times the distance in comparison to the vertical path through the atmosphere. The Figure 3 shows the spectrum outside the atmosphere (AM 0) and at the surface of the Earth (AM 1.5). The spectrum describes the composition of the light and the contribution of the different wavelengths to the total irradiance.

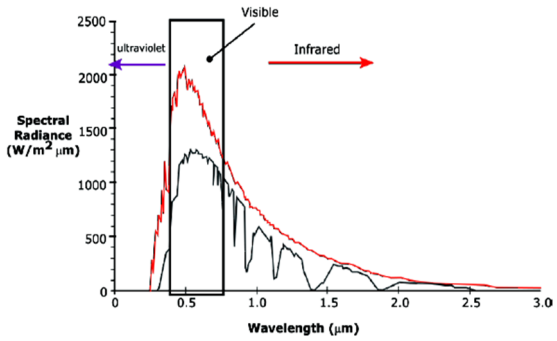

Figure 2. AM0 and AM1 spectrum, at sun height of 41,8° [7].

Some characteristics of the solar spectrum are:

- The 7% of irradiation outside the atmosphere, i.e. the AM0, falls in the ultraviolet range and the 47% falls in the visible range.
- The AM 1.5 spectrum is reduced due to the absorption.

Because of the existence of many companies and laboratories that develop solar cells and photovoltaic systems, it is necessary to establish the conditions with which comparing the performance of the different solar cells and photovoltaic modules. These conditions are the standard test conditions(STC), characterized by:

- Irradiance of 1 367W.m^{-2}
- AM1.5 spectrum
- and a cell temperature of 25° C.

The AM1.5 is defined in the International Standard IEC 60904-3[8]. STC and the AM 1.5 spectrum are used all over the world in industry and laboratories.

The incident radiation from the sun is the basis for all life on the Earth. Solar energy generation is the availability of transform sun light into any other form of energy, e.g. green plants, and some other organisms use sunlight to synthesize foods from carbon dioxide and water in a process called photosynthesis. Humans cannot directly transform the energy, but we use devices to mechanically or chemically convert it.

Photovoltaic energy conversion in general words can be explained as the technology that generates electrical power measured in Watts(W) from semiconductors when they are illuminated by photons [9].

The work is focused on to get the optical and electrical characteristics of two-dimensional(2D) single junction GaAs solar cell by using numerical simulations to develop and optimize semiconductor processing technologies and devices by means of *Sentaurus Technology Computer-Aided Design* (TCAD) [10] tools.

The process starts defining the geometrical structure and materials, then we obtain the generation profiles and insert those result in a process, called V isual, that extracts and filters the data to show graphics, curves, band diagrams and profiles of the figures of merit to evaluate the solar cell performance. Finally, in order to get an optimized GaAs solar cell, additional simulations have been done, changing the geometric and doping levels of the layers of the cell.

The simulated electrical characteristics include the light current–voltage (I–V) characteristics (using AM1.5 solar spectrum) and the energy band diagram. The optical characteristics that are obtained are the reflectance spectra, the spectral current densities and the quantum efficiency spectra (at short-circuit current density).

1.3 Photovoltaic energy convertion in a GaAs solar cell

As we know, a solar cell structure consists of an absorber layer, in which the photons of an incident radiation are efficiently absorbed resulting in a creation of electron-hole pairs. In order to separate the photogenerated electrons and holes from each other, the socalled “semi-permeable membranes” are attached to the both sides of the absorber [11].

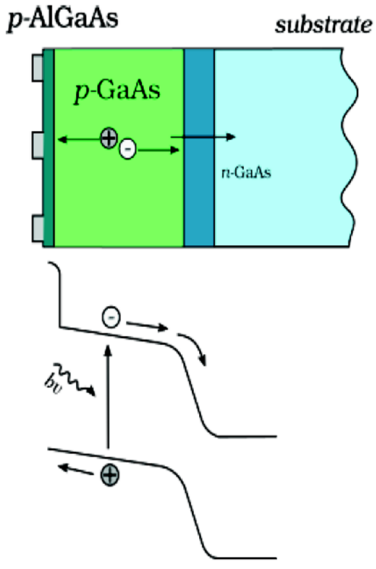

Figure 4. Photovoltaic effect in a GaAs solar cell.

A gallium-arsenide (GaAs) solar cell have a passivating Alluminum Gallium Arsenide (AlGaAs) layer that covers the top surface and prevents the surface recombination of minority carriers (electrons) from the emitter but transmits most of the incident light in the emitter layer where most of the power is generated, as sketched in figure 4.

1.4 GaAs Solar cell features

Solar cell based in *AlGaAs-GaAs* alloys are used at high-efficiency, they are related with the semiconductors of the III-V group, because these are made with compounds of elements from the column III and V in the periodic table. *GaAs* is alloyed with *Al* to give the ternary compound $Al_xGa_{1-x}As$; compound that was analized and simulated in this paper.

The characteristics of Gallium Arsenide (GaAs) have made of it, a photovoltaic material of interest. The bandgap of GaAs is 1.42 eV at 300K. This is very nearly ideal for a photovoltaic device operating in our solar spectrum. Therefore, GaAs solar cells can operate at higher temperatures than silicon (Si) cells and are expected to be very radiant resistant, furthermore GaAs solar cells have higher electron mobility and higher saturation velocity [12].

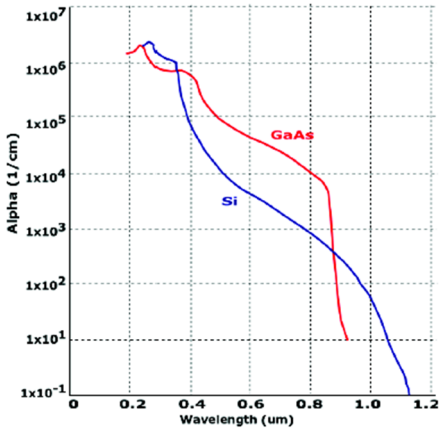

Figure 5. Photovoltaic effect in a GaAs solar cell.

The direct bandgap of the GaAs causes in the material a high optical absorption coefficient. This coefficient indicates how far the light of a particular wavelength can penetrate before that it have been absorbed. In a material with a low absorption coefficient, light is poorly absorbed, additional if the material is thin, it can be seen as a transparent layer [12]. The for GaAs rises very steppy at the band edge (λ= 0,88μm) to values grater than $104cm^{-1}$, in contrast with the gradually rise of the absorption coefficient for silicon. We can see the curves of optical absorption vs. wavelength for the both of materials in figure 5.

About GaAs solar cells, there are some investigations with several techniques and processes to study the cells. In [13] an introduction to the concept of optical coupling matrix is presented, to account a photon recycling effects in a numerical model of a GaAs solar cell. Therefore, some techniques to separate a III–V solar cell structure from its underlying GaAs, are presented in [14].

1.5 Simulation software

Sentaurus is a TCAD software, developed by Synopsys, which solves the diffusion and transport equations, to modeling the structural properties and electrical behavior of semiconductor devices. All leading semiconductor companies use Synopsys TCAD tools throughout the technology development cycle. TCAD tools allow engineers to explore new design alternatives, test the quality of passivation layers, varying the lifetimes of charges executing simulations. Also is possible to evaluate, characterize, and optimize the process.

2. GaAs solar cell based analysis

In 1970 a Russian group reported a heterojunction solar cell consisting of a p-type emitter of $Ga_{1-x}Al_xAs$, grown on a *n-type* base of GaAs. It means that the layer can be made thick and heavily doped reducing the series resistance and reduce the surface recombination [12].

The solar cell that is analyzed and simulated is a GaAs based. It use two layers of an antireflective coating (ARC), the first one is a MgF2 layer and the second one a TiO_2 layer. The bulk is GaAs based with two differents levels of doping, dividing the bulk in a emitter and a base. The caracteristics ans parameters for each material are introduced in the *sdevice* script of the software. To reduce the recombination losses, a front surface field (fsf), is used, and a back surface field (bsf) made of AlGaAs. A preliminary sketch of the solar cell is shown in figure 6.

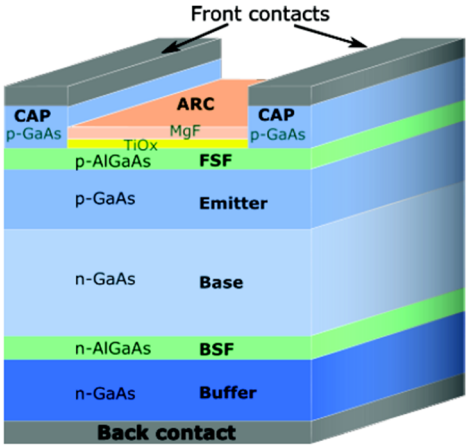

Figure 6. Schematic of the GaAs solar cell. Electrons and holes are extracted through the front contact and the back contact.

2.1 The architecture of GaAs-AlGaAs solar cell

TCAD simulator requires some dimensions: lengths, shape geometry, mesh, and doping profiles. The bandgap of GaAs is close to the optimum Eg for single junction solar cells whose maximum efficiency is above 30% [15]. A sketch of the model is shown in figure 6.

Note that the structure has been studied under AM1.5 solar spectrum, with P=0,1W/cm^2, and at room temperature T = 300K.

The GaAs solar cell structure includes a ”buffer layer” of *n-doped* GaAs, even though such a buffer layer is not needed theoretically. It was been included for practical reasons, because the doping level and the surface quality of the GaAs wafer actually available have been found to lack adequate control. Furthermore, the higher n+ doping level in the GaAs substrate rather than in the n- doped buffer layer allow easier fabrication of the back contact. The important characteristics for GaAs cells are: a thin (AlGaAs) fsf layer less than 0,5 µm and a diffused electrical junction less than 0,5 µm deep.

This ensures low optical absorption losses and minimizes the surface-recombination characteristic of GaAs surfaces and the latter ensures increased radiation hardness [17]. The detail of thickness and doping levels from figure 6, used for simulations are specified in table 2.

2.2 Simulation domains and mesh definition

The method of simulation adopted for this work consists in evaluate independently the optical and electric simulations. For instance, the meshing resolution

Table 2. Details of solar cell structure to simulate

Region	Material	Thickness(µm)	Doping(cm^{-3})
cap	GaAs	0,2	-1,00e^{19}
fsf	AlGaAs	0,04	-2,00e^{18}
emitter	GaAs	0,8	-9,00e^{17}
base	GaAs	3,2	1,00e^{17}
bsf	AlGaAs	0,2	5,00e^{18}
buffer	GaAs	0,35	2,00e^{18}
contacts	Aluminium	1	

size should be much finer than the needed to solve the electrical behavior, in the device. Even the considerations of sizing and shape are different for each one. Regarding the optical analysis, it is important considering the effects of surface texturing over the charge collection but is sufficient enough to take a look only in a portion that characterized the full surface roughness instead of unnecessary modeling the whole device area. Taking the case of a solar cell featuring finger as front contact and a back contact in the whole rear, it is sufficiently just modeling a small respective portion of the structure, that is typically half of the symmetry element in two dimensions, and a quarter of the symmetry element in three dimensions as is shown in figure 7.

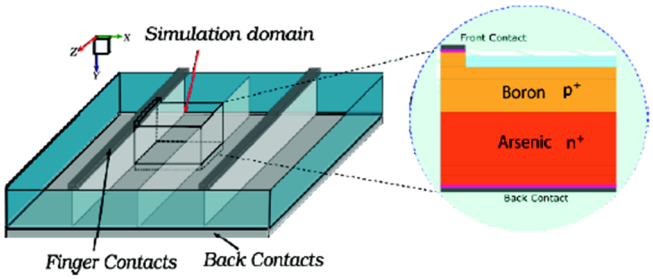

Figure 7. Simulation domain. Left side, 3D simulation domain selection. Right side, 2D resulting simulation domain.

The electric-simulation domain is usually bigger than the optical one and requires another meshing strategy. The meshing procedure starts by creating a coarse grid in the whole structure followed by the addition of finer meshing refinements near to the junctions and metal contacts, as well as, in the uppermost part of the device, where most of the generation occurs. In figure 8, is

sketched a mesh for the simulation domain from figure 7.

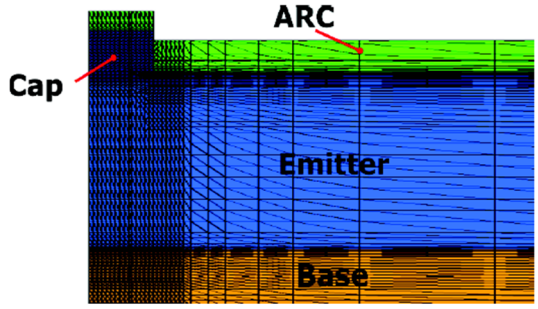

Figure 8. Mesh definition for a piece of the simulation domain.

3. Optical simulation results

In order to obtain the optical characteristics in the simulation, we have to calculate the topics listened below:

- Optical intensity, absorbed photon density and optical generation rate using TMM solver.
- Optical intensity, absorbed photon density and optical generation rate using Raytracing solver.
- Integrated optical generation rate, which is used subsequently in Sentaurus Visual to compute the photogenerated current density *Jph(mA/cm^2)*.
- Reflectance, transmitance and absorbance.
- Terminal current density *J(mA/cm^2)*

3.1 Optical generation profiles

Simulation of PV devices under illumination requires a source file numerically coupling, by Sentaurus TCAD, to the simulation domain that contains the geometry structure, mesh and optical physics information of materials to calculate the photogeneration rate of electron-hole pairs by solving the transport equations. The solar spectrum file sweeps the wavelength of incident sunlight from (300 nm) up to (1200 nm) using the conventional one-sun AM1.5d spectrum with an incident power of 1000 W.m^2, defined in a file with two-columns format. The first column contains the wavelength in μm and the second one contains the intensity in Wcm^{-2}. This file is calculated based on the air mass 1.5 global tilted irradiance, by the spectral radiation model called SMARTS v 2.9.2 with inputs chosen per international standard IEC 60904-3-Ed2 [18], as shown in figure 9. The simulator also calculates the reflectance, transmittance, and absorbance as a function of the wavelength (λ).

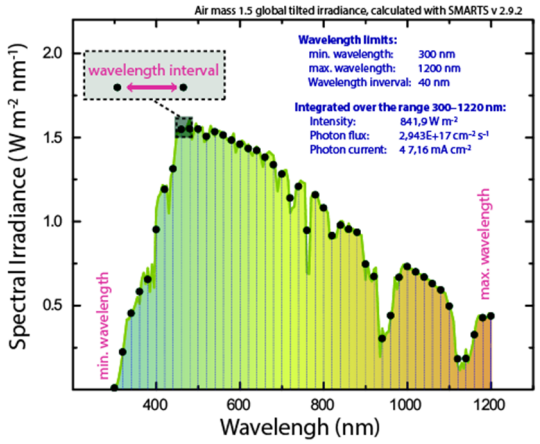

Figure 9. Air mass 1.5 global tilted irradiance.

The absorption coefficient is computed from and Wavelength (λ) according to $\alpha = (4\pi/\lambda).k$. It determines how far inside a material the light, with a particular wavelength, can penetrate before being absorbed to create electron-holes pairs. Semiconductor materials can only absorb energy from particles that have sufficient energy to excite an electron from the valence band to the conduction band.

3.2 Optical results using the Transfer Matrix Method (TMM)

The TMM solver computes the optical intensity by taking into account the interference effects due to standing waves or by neglecting the phase and, therefore, the interference effects. Neglecting the phase is valid only for large layer thicknesses (depending on the extinction coefficient). It is assumed, in the model of the optical generation rate, monochromatic plane waves with arbitrary angles of incidence and polarization states penetrating a number of planar, parallel layers.

These matrices are functions of the complex wave impedances *Zj* given by $Zj=nj.cos(\theta j)$ in the case of E polarization (TE) and by $Zj = nj/cos(\theta j)$ in the case of H polarization (TM). Here, *nj* denotes the complex index of refraction and θj is the complex counterpart of the angle of refraction ($n_0.sin(\theta_0)=nj.sin(\theta j)$).

In the figures 10 and 11, are presented the optical generation rate and the optical generation profile in GaAs solar cell as a function of depth.

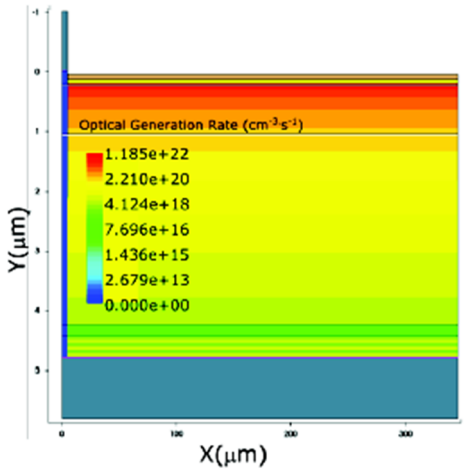

Figure 10. Optical generation rate for a full metallized rear contact.

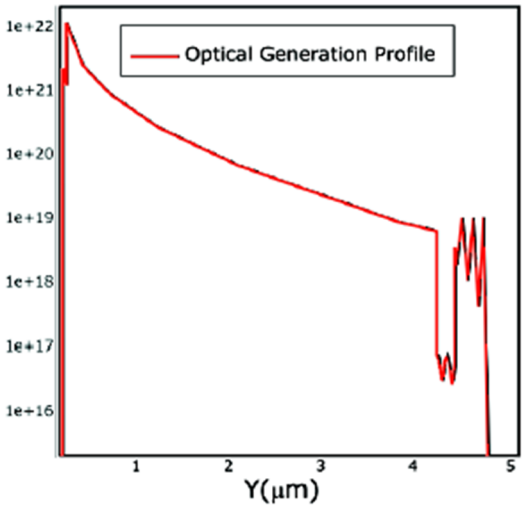

Figure 11. Optical generation profile for a full metallized rear contact.

Two simulations have been done, one for the case in which the whole rear surface is completely metallized, figure 10 and figure 11, and the others for the case which considers a rear contact of *5μm*, as shown in figures 12 and 13.

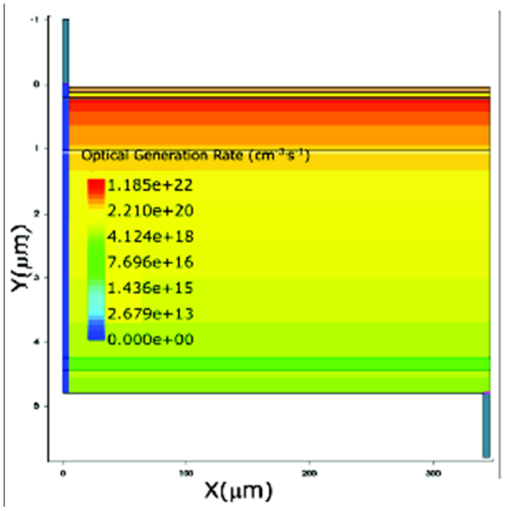

Figure 12. Optical generation rate for a 5um rear contact.

The blue-colored region below the front contact finger indicates that the optical generation rate is zero in the region since it is not illuminated. The optical generation profile shows that the optical generation rate decreases as a function of depth.

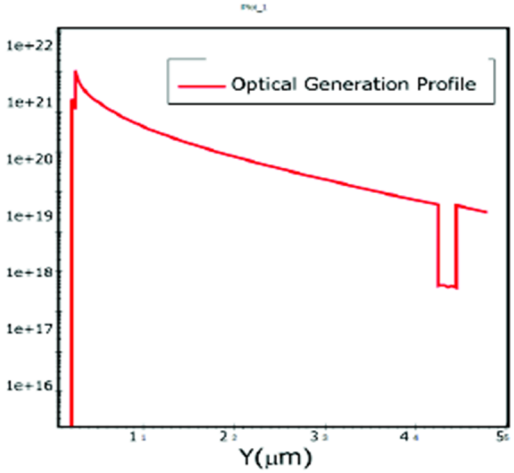

Figure 13. Optical generation profile for a 5um rear contact.

In both of the results we have present the effect of the bsf as a hole at the end of the curve. In the case of full metallized rear contact, it presents the effect of a full aluminum metallized rear contact as a kind of perturbations near to the back contact. In the other case, the effect of the rear contact is almost imperceptible.

In order to have a confront between the two optical generation profiles, the data is then post process using Matlab. The figure 14 shows the confront between the two optical generation profiles.

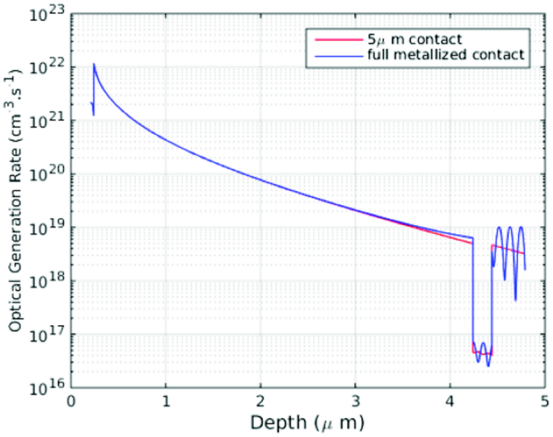

Figure 14. Optical generation profiles TMM-based.

3.3 Optical results using the "Raytracer" algorithm

In the section of the simulator called Sentaurus Device, each material has a complex refractive index section defined in the parameter file. The raytracer solver uses a recursive algorithm that starts with a source of rays and it builds a binary tree that tracks the transmission and reflection of the rays. A reflection-transmission process occurs at interfaces with refractive index differences. The obtained results are shown in figures 15, 16, 17 and 18.

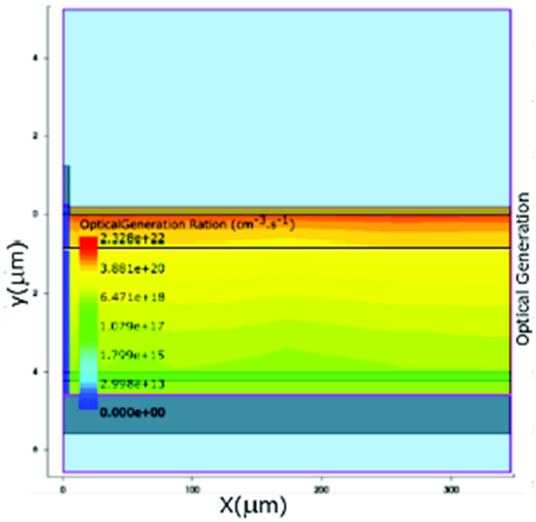

Figure 15. Optical generation rate for a ful metalized rear contact. Raytracing method.

In the region over and under the cell there are also simulated the pieces of ambient that are used as sensor for the rays. The rays starts at a height of 2,5μm over the cell.

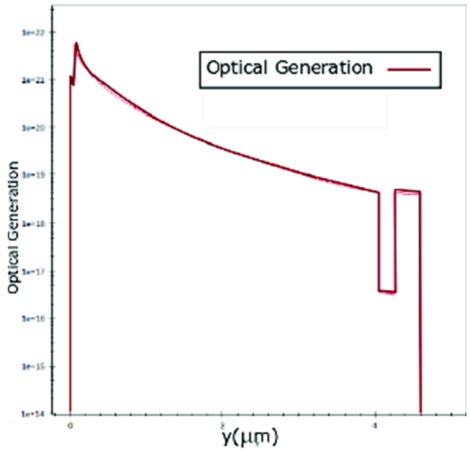

Figure 16. Optical generation rate for a ful metalized rear contact.

The results of Raytracing are in the same range that the results of the TMM process. With this results we can say the both of the methods can work for the model of solar cell under the optical analysis. In the Raytrace 2D simulation there are oscillations and random values of optical generation due to the nature and behavior of the incident rays. Finally, in order to have the effect of the metalization on the cell, a confront between the optical generation with full metalized back contact and the contact of 5um, is presented.

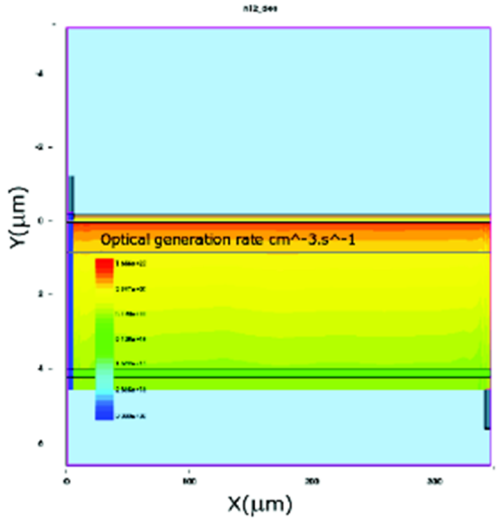

Figure 17. Optical generation rate for a 5um rear contact.

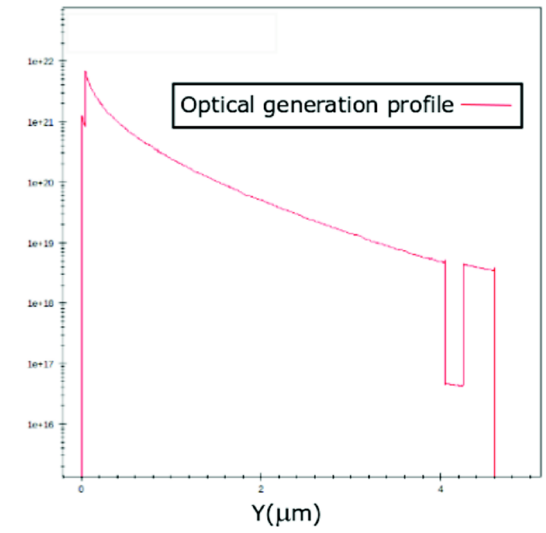

Figure 18. Optical generation profile for a 5um rear contact.

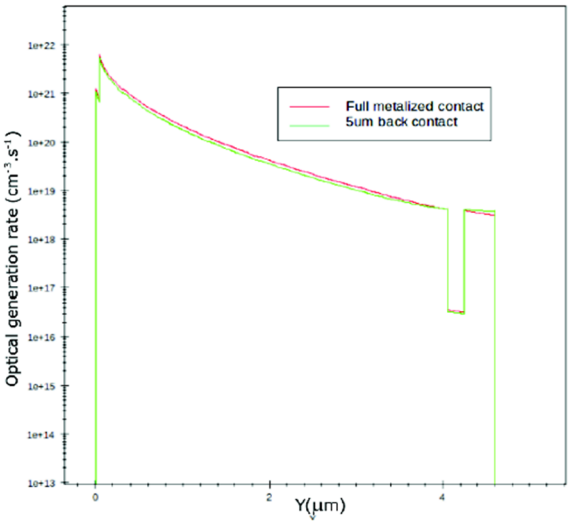

Figure 19. Optical generation between the full metalized back contact against 5um back contact.

4. Electrical simulation results

The I–V characteristics of the illuminated solar cell are simulated by ramping the anode voltage. There are two ramps, the goal voltage for the first ramp should be less than Vmpp. The goal voltage for the second ramp should be greater than *Voc*. Since both P_{mpp} (and, therefore, V_{mpp}) and *Voc* are unknown before starting the simulation, the goal voltages for both ramps are chosen iteratively. Initially, the simulation runs with a guessed value of V_{mpp} and then looks at the computed P–V characteristics to establish a better approximation or V_{mpp}.

4.1 Impact of the total width in the solar cell

The first attempt to optimize the model is to change the total pitch of the cell, to determine the best width to continue with the others optimization changes. Figure 20 shows the efficiency and FF against the length of the pitch. According to figure 20, the best length is *325um*, the efficiency tend to go up until the *325um*. Around the *325um* the efficiency becomes constant but the Fill Factor decreases, as show in figure 21.

The best trade-off between the conversion efficiency and the Fill Factor FF take place at a total width of *325um.*

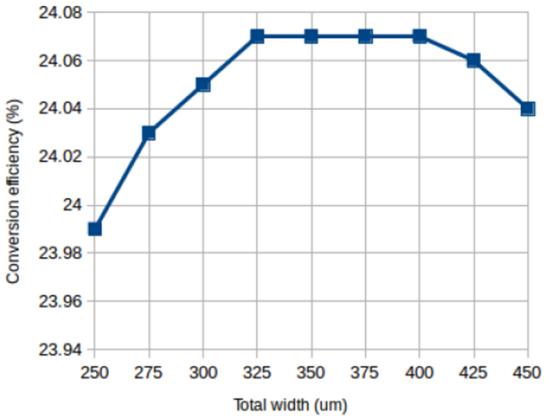

Figure 20. Convertion effiency vs Cell width.

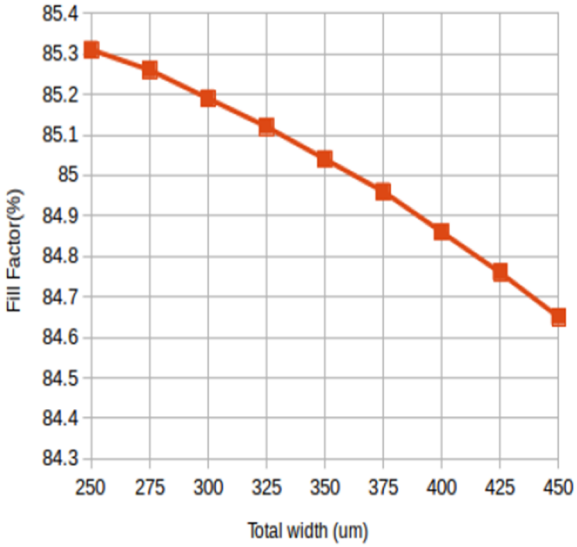

Figure 21. Effect of the width in the solar cell performance.

4.2 Impact of the FSF layer in the solar cell

The Figure 22 shows the behavior of J_{sc} as a function of the *AlGaAs fsf* layer thickness, in order to determine the advantage of using thin FSF layers.

Two different experiment have been done about the FSF layer, one rewarding the doping of the layer and the other one changing the thickness of the fsf layer, figure 23.

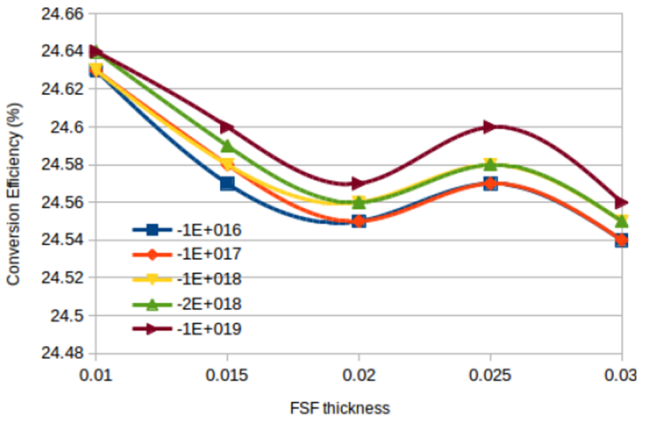

Figure 22. Conversion efficiency.

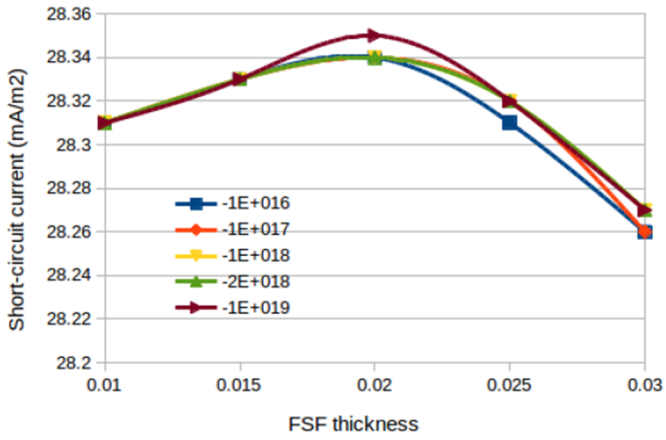

Figure 23. Short-circuit current.

4.3 Impact of the base layer

To study the influence of the base layer,the thickness of the latter is varied between 1µm and 9µm [19] and the doping level from $1x10^{16}cm^{-3}$ to $2x10^{16}cm^{-3}$. The other parameters are configured as shown in table 3.

Table 3. Layer configuration for the GaAs solar cell

Region	Cell width(µm)	Thickness(µm)	Doping(cm^{-3})
cap	5	0,2	$-1{,}00e^{19}$
fsf	325	0,04	$-2{,}00e^{18}$
emitter	325	0,8	$-9{,}00e^{17}$
bsf	325	0,2	$5{,}00e^{18}$
buffer	325	0,35	$2{,}00e^{18}$

According to the figure 24, the best conversion efficiency is around 2µm, but depending on the doping, it has different values. For a doping level of 1e+16 we have an efficiency around 22,5%. Then with a doping level of 2e+17 and the thickness of 2µm the conversion efficiency of the cell arrives to his maximum value, 24,7%. But if the doping continues to increment, the efficiency decrements, as the example, with a doping level of 5e+17 the efficiency is 23,5%.

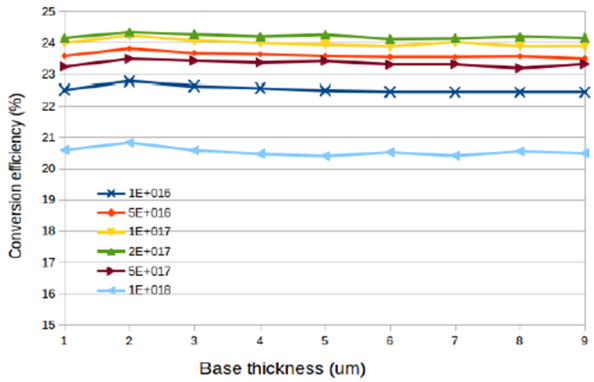

Figure 24. Base thickness effect.

Photons with lower energy which are absorbed with base layer are sensitive to the layer thickness and absorption coefficient. The base layer thick is 2µm, enough to absorb as much photons as possible and lower doing concentration level in order to improve the collection of photo-generated carriers. Figure 21 shows the effect of doping level on the conversion efficiency.

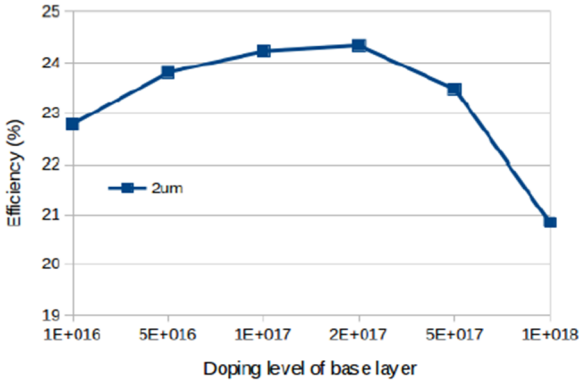

Figure 25. Base doping level effect.

4.4 Impact of the Emitter layer

In one hand, the intention of the heavily doping in the emitter layers is to improve its conductivity. But, in the other hand, the thickness of the base and the emitter should exceed the incident photon's absorption length. Figures 26 and 27 show the efficiency versus the doping and thickness of the emitter layer. The doping concentration level of the base and the emitter thickness change quickly the efficiency of the cell.

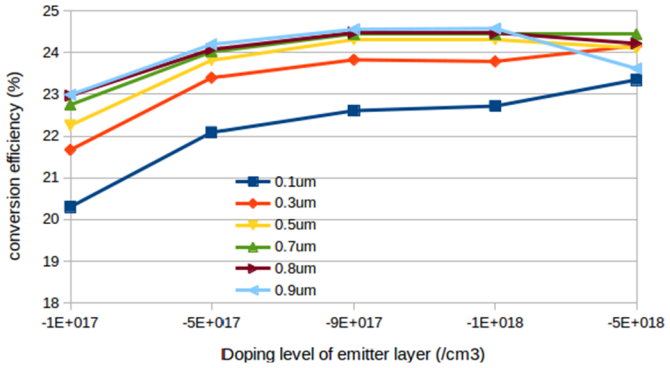

Figure 26. Emitter doping level effect.

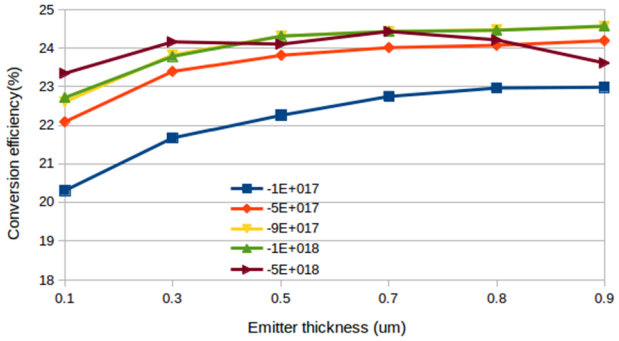

Figure 27. Thickness of emitter effect.

5. Optimized model

The optimized geometrical parameter and the results are presented in the table 4 and table 5, respectively.

Table 4. Optimized GaAs solar cell results

Region	Layer width(µm)	Thickness(µm)	Doping(cm^{-3})
cap	5	0,2	-1,00e^{19}
fsf	325	0,02	-2,00e^{18}
emitter	325	0,9	-1,00e^{18}
bsf	325	0,2	5,00e^{18}
buffer	325	0,35	2,00e^{18}

Rear contact width (um)	Jsc (mA/cm^2)	Voc(V)	Jph (mA/cm^2)	FF(%)	η(%)
5	28,27	1,024	29,01	84,56	24,47
325	28,3	1,023	29,01	84,85	24,58

5.1 Light J-V characteristics

The I-V and P-V characteristics of the illuminated cell are presented in Figure 28. The power density of the cell is also computed using $P = JV$. The fill factor and the power conversion efficiency are also computed. The obtained values for the 2D optimized cell, considering the full metalized contact approach are, $Jsc = 28{,}3mA/cm^2$ and $Jph = 29{,}09mA/cm^2$, instead of, for the *5um* back contact approach, the results are, $Jsc = 28{,}27mA/cm^2$ and $Jph = 29{,}01mA/cm^2$. The value of $Jsc<Jph$ because all the photon generated carriers cannot be collected at the electrodes, due to recombination losses.

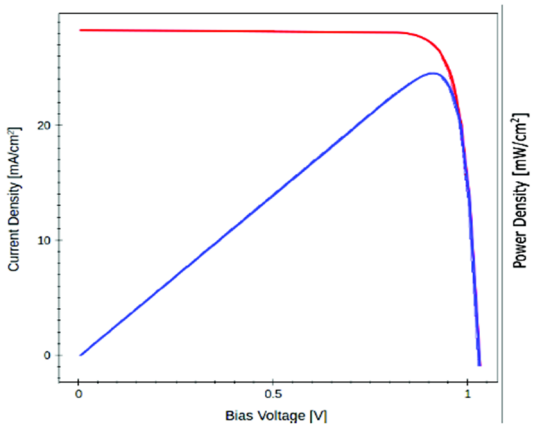

Figure 28. Light I-V and P-V characteristics of full metalized back contact GaAs solar cell.

5.2 Energy band diagram

The energy band diagram of the solar cell is plotted using the conduction band energy, the valence band energy and the electron and hole quasi-Fermi energies from the *Plot* section in the *sdevice* Senturus'script. The Figure 29, shows the band diagram for the optimized GaAs solar cell at the short-circuit current density.

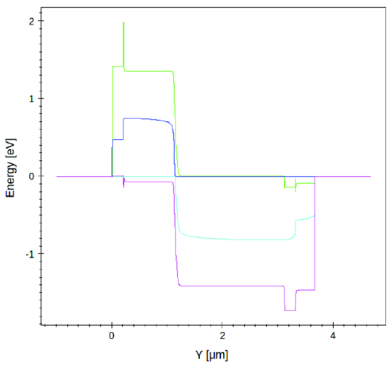

Figure 29. Energy band diagram of GaAs solar cell at short circuit current density.

6. Conclusions

TCAD modeling is a powerful and helpful tool that reduce the time of manufacturing and speed up the optimization processes of solar cell. It allows test the concept designs before the implementation, improve the old ones or simply optimized a designed model. An optimized AlGaAs-GaAs solar cell was designed. The two approaches, were simulated. The first one, considered a full metallized back contact and the second one using a smaller back contact of 5µm in order to be implemented as a top cell in a tandem solar cell approach. Some special characteristics that makes this kind of cells specials are the high efficiency and the capability to develop thinner lower weight solar cells.

Two important characteristics are needed for GaAs solar cell, a thin AlGaAs fsf layer less than 0,5µm thick and a diffused electrical junction less than 0,5µm deep, to ensure optical absorption losses and minimizes the surface recombinations. The characteristics of the full metalized back contact are better because of the bigger area of the back contact to collect electrons.

7. References

[1] K. Mertens, Photovoltaics: Fundamentals, technology and practice. John Wiley & Sons, 2013.

[2] Viorel, B. (2008). Modeling solar radiation at the earth's surface: recent advances.

[3] C. Zhang, High Efficiency GaAs-based Solar Cells Simulation and Fabrication. Arizona State University, 2014.

[4] Kerker, M. (2013). The scattering of light and other electromagnetic radiation: physical chemistry: a series of monographs (Vol. 16). Academic press.

[5] Naqvi, Zeba & Green, Mark & Smith, Krista & Wang, Chaofan & Del'Haye, Pascal & Her, Tsing-Hua. (2018). Uniform Thin Films on Optical Fibers by Plasma-Enhanced Chemical Vapor Deposition: Fabrication, Mie Scattering Characterization, and Application to Microresonators. Journal of Lightwave Technology. 10.1109/JLT.2018.2876026.

[6] List, R. J., Ed. 1951. Smithsonian Meteorological Tables. 6th rev. ed., p. 422.

[7] A. Luque and S. Hegedus, Handbook of photovoltaic cience and engineering. John Wiley & Sons, 2011.

[8] I. E. Commission et al., "Standard iec 60904-3: Photovoltaic devices,"Part 3: Measurement Principles for Terrestrial Photovoltaic (PV) Solar Devices With. Reference Spectral Irradiance Data, 1987.

[9] S. S. Hegedus and A. Luque, "Status, trends, challenges and the bright future of solar electricity from photovoltaics," Handbook of photovoltaic science and engineering, pp. 1–43, 2003.

[10] "TCAD." Software Integrity, Retrieved from www.synopsys.com/silicon/tcad.html.

[11] P. Würfel, Physics of solar cells-from principles to new concepts. 2005.

[12] The absorption of radiation in solar stills," Solar Energy, vol. 12, no. 3, pp. 333 –346, 1969,
, ISSN: 0038-092X.

[13] G. Letay, M. Hermle, A.W. Bett, "Simulating single-junction GaAs solar cells including photon recycling", Progress in Photovoltaics: Research and Applications 14, 683 (2006).

[14] G.J. Bauhuis et al., 26.1%thin-filmGaAs solar cell using epitaxia lift-off, Solar Energy Materials & Solar Cells 93 (2009) 1488–1491.

[15] R Loo, G. Kamath, and R. Knechtli, "Radiation damage in gaas solar cells," 1980.

[16] C. Zhang, High Efficiency GaAs-based Solar Cells Simulation and Fabrication. Arizona State University, 2014.

[17] R Loo, G. Kamath, and R. Knechtli, "Radiation damage in GaAs solar cells," 1980.

[18] C. Gueymard, SMARTS2: A simple model of the atmospheric radiative transfer of sunshine: Algorithms and performance assessment. Florida Solar Energy Center Cocoa, FL, 1995.

[19] M Abderrezek, F Djahli, M Fathi, and M Ayad, "Numerical modeling of gaas solar cell performances," Elektronika ir Elektrotechnika, vol. 19, no. 8, pp. 41–44, 2013.